MULTI-AGENT 3D SEISMIC EXPLORATION USING ADAPT-THEN-COMBINE FULL WAVEFORM INVERSION IN A HARDWARE-IN-THE-LOOP SYSTEM

Ban-Sok Shin, Dhruv Patel, Luis Wientgens, Kai Nierula, and Dmitriy Shutin

German Aerospace Center (DLR)
Institute of Communications and Navigation
E-Mail: {ban-sok.shin, dhruv.patel, luis.wientgens, kai.nierula, dmitriy.shutin}@dlr.de

ABSTRACT

We present a 3D seismic exploration and imaging survey conducted by robotic platforms in a hardware-in-the-loop system. To this end, we integrate the adapt-then-combine full waveform inversion (ATC-FWI) over a network of mobile rovers in the ROS2 framework. The ATC-FWI allows for distributed subsurface imaging in a multi-agent network, i.e., each rover obtains a 3D subsurface image via data exchange with other rovers in the network. We demonstrate the capability of our system by performing multiple surveys using a synthetic subsurface model with an anomaly. The rovers acquire seismic data over different measurement areas and perform distributed imaging to reconstruct the subsurface. We show that the rovers are able to image the anomaly and to enhance their subsurface image over multiple measurement stages in different areas.

Index Terms— Robotic seismic exploration, multi-agent systems, distributed imaging, full waveform inversion

1. INTRODUCTION

In recent space exploration missions, acquisition of seismic data from extraterrestrial planets such as Mars has become increasingly relevant [1]. Usually, a single rover equipped with a variety of different sensors is employed that explores a certain terrain of the respective planet. Nowadays, these rovers carry a sensor to obtain information about the subsurface: Either a seismometer or a ground penetrating radar [2, 3]. For future planetary exploration one envisions the use of multiple robots which perform exploration tasks in an autonomous fashion [4], e.g. in our case a seismic survey [5]. Here, the rovers are equipped with geophones to measure seismic data. An active, mobile source is used to inject seismic waves into the ground. Furthermore, the rovers are connected to each other over wireless links to enable data exchange within the network. Such connectivity is also used to localize the rovers over the wireless links in a completely distributed fashion [6]. No central entity is used that controls the multi-agent network but rather the network itself is to carry out the survey. The objective is to image the subsurface within the network of agents such that each agent obtains a subsurface image locally. Based on this image the agents shall optimize their sampling positions to enhance the subsurface image.

One key enabler for the realization of such a system is *distributed seismic imaging*. This method allows to obtain subsurface images at each rover locally by cooperation with other rovers in the network. The authors have proposed distributed imaging methods in the past [7, 8]. In particular, a distributed implementation of the full waveform inversion (FWI) based on the adapt-then-combine (ATC) technique has been proposed. The so-called ATC-FWI enables a distributed subsurface imaging within a multi-agent network that performs close to its centralized counterpart, the traditional FWI. With this technique each rover is able to obtain an estimate of the subsurface image locally via cooperation with neighboring agents only.

We describe a hardware-in-the-loop (HIL) implementation of the ATC-FWI using mobile rovers. These rovers carry a Raspberry Pi 4 (RPi4) on which the ATC-FWI is implemented. To generate seismic measurements at the rovers we employ a numerical solver of the 3D acoustic wave equation. To simulate a robotic seismic survey the rovers move over the complete exploration area performing measurements and imaging at predefined locations. The data exchange among rovers required in ATC-FWI is emulated by a central access point that routes the data to the respective rovers. To demonstrate the functionality of our HIL system we conduct several experiments using a 3D synthetic subsurface model. We show that our HIL is able to image a subsurface anomaly at each rover using ATC-FWI.

2. 3D ADAPT-THEN-COMBINE FULL WAVEFORM INVERSION

We give a brief overview of the full waveform inversion (FWI) and the adapt-then-combine full waveform inversion (ATC-FWI) as a distributed implementation of the FWI.

FWI is a geophysical imaging technique that obtains high-resolution subsurface images based on seismic data [9, 10]. In its simplest form FWI considers a least-squares cost between observed seismic data $\boldsymbol{d}_{\mathrm{obs}} \in \mathbb{R}^{N_{\mathrm{T}} N_{\mathrm{R}}}$ and synthesized data $\boldsymbol{d}_{\mathrm{syn}}(\boldsymbol{m}) \in \mathbb{R}^{N_{\mathrm{T}} N_{\mathrm{R}}}$ for a measurement time of N_{T} samples and N_{R} receivers. The synthesized data is generated using an estimated subsurface model $\boldsymbol{m} \in \mathbb{R}^{N_x N_y N_z}$ where N_x, N_y, N_z denote the number of spatial grid points in x, y, z-dimension, respectively. In our case, the subsurface model $\boldsymbol{m}$ consists of scalar values that represent the P-wave velocity at a spatial coordinate $\boldsymbol{x} = (x, y, z)$. The observed data $\boldsymbol{d}_{\mathrm{obs}}$ contains the sampled waveforms measured over time of all N_{R} receivers/geophones. The cost in classical FWI reads

$$\mathcal{L}(\boldsymbol{m}) = \frac{1}{2} ||\boldsymbol{d}_{\mathrm{obs}} - \boldsymbol{d}_{\mathrm{syn}}(\boldsymbol{m})||_2^2. \tag{1}$$

To synthesize data $\boldsymbol{d}_{\mathrm{syn}}(\boldsymbol{m})$ at the receiver positions the wave equation needs to be solved. To this end, the acoustic wave equation can be used if one considers P-wave propagation only:

$$\frac{1}{\boldsymbol{m}^2(\boldsymbol{x})} \frac{\partial^2 \boldsymbol{u}(\boldsymbol{x}, t)}{\partial t^2} - \frac{\partial^2 \boldsymbol{u}(\boldsymbol{x}, t)}{\partial \boldsymbol{x}^2} = \boldsymbol{f}(\boldsymbol{x}, t). \tag{2}$$

Here, variable $\boldsymbol{u}(\boldsymbol{x}, t)$ is the acoustic wavefield over space $\boldsymbol{x}$ and

The work leading to this publication was partially funded by the German Research Foundation (DFG) under grant SH 1975/1-1.

time t while $\boldsymbol{f}(\boldsymbol{x}, t)$ denotes the source term, e.g., a hammer strike or explosive. The objective is then to minimize $\mathcal{L}(\boldsymbol{m})$ with respect to (w.r.t.) the subsurface model $\boldsymbol{m}$ subject to the constraint (2). To this end, FWI considers iterative minimization schemes and uses the adjoint-state method [11] to obtain the gradient of $\mathcal{L}(\boldsymbol{m})$ w.r.t. $\boldsymbol{m}$. Details on how to compute the gradient can be found in [7]. Using steepest-descent the subsurface model $\boldsymbol{m}$ is then updated via gradient descent as $\boldsymbol{m} \leftarrow \boldsymbol{m} - \alpha\, \boldsymbol{m}_\Delta$ with $\boldsymbol{m}_\Delta$ being the gradient and $\alpha > 0$ being a step size.

To apply FWI to a multi-agent seismic survey, we consider a distributed implementation. We assume that each agent r carries a seismic receiver or geophone to acquire seismic data and that the agents are connected to each other over wireless links. Furthermore, each agent r can exchange data with agents ℓ that are connected to it. These connected agents are contained in a neighborhood set $\mathcal{N}_r$ that also includes the agent r itself. Furthermore, all agents are contained in the set $\mathcal{R} = \{1, \ldots, N_\mathrm{R}\}$ and we assume a connected graph w.r.t. the topology of the multi-agent network.

The goal of distributed subsurface imaging is to obtain an estimate $\boldsymbol{m}$ of the subsurface at each agent via cooperation among these. To this end, the FWI cost in (1) is separated over the agents $\mathcal{R}$:

$$\mathcal{L}(\boldsymbol{m}) = \frac{1}{2}||\boldsymbol{d}_\mathrm{obs} - \boldsymbol{d}_\mathrm{syn}(\boldsymbol{m})||_2^2 = \sum_{r\in\mathcal{R}} \mathcal{L}_r(\boldsymbol{m}) \tag{3}$$

where $\mathcal{L}_r(\boldsymbol{m}) = \frac{1}{2}||\boldsymbol{d}_{\mathrm{obs},r} - \boldsymbol{d}_{\mathrm{syn},r}(\boldsymbol{m})||_2^2$ is the local cost of agent r, i.e., it considers the data residual based on observed data from agent r only. Using the local cost $\mathcal{L}_r(\boldsymbol{m})$ each agent r computes a local gradient $\boldsymbol{m}_{\Delta,r}$ with the adjoint-state method, i.e., $\boldsymbol{m}_{\Delta,r} = \nabla_{\boldsymbol{m}} \mathcal{L}_r(\boldsymbol{m})$, cf. [7]. We then apply the adapt-then-combine (ATC) technique [12] to obtain a distributed FWI:

$$\text{(Adapt)} \quad \widetilde{\boldsymbol{m}}_r \leftarrow \boldsymbol{m}_r - \alpha \sum_{\ell\in\mathcal{N}_r} c_{\ell r} \boldsymbol{m}_{\Delta,\ell} \tag{4a}$$

$$\text{(Combine)} \quad \boldsymbol{m}_r \leftarrow \sum_{\ell\in\mathcal{N}_r} a_{\ell r} \widetilde{\boldsymbol{m}}_\ell \tag{4b}$$

The coefficients $c_{\ell r}$ and $a_{\ell r}$ are weighting factors for the respective averaging procedures and need to be chosen accordingly to guarantee convergence of the algorithm. Details on selection of these coefficients can be found in [7, 13]. The ATC technique enables each agent to obtain a subsurface image that resembles the global result, i.e., when all data are available at a central entity and FWI is performed. Eq. (4) builds the so-called ATC-FWI. In each iteration, gradients $\boldsymbol{m}_{\Delta,\ell}$ and intermediate models $\widetilde{\boldsymbol{m}}_\ell$ need to be exchanged among neighboring agents.

3. HARDWARE-IN-THE-LOOP SYSTEM DESIGN

In the following, we describe the basic architecture of our (HIL) system and its main components. As robotic platforms we employ four small custom built track based rovers. These rovers are controlled using the Robot Operating System 2 (ROS2 Foxy, [14]) on a RPi4 Module carried by the rovers. The exploration area is covered by a Vicon system with 25 cameras which provides ground-truth data of the respective rover positions. To move the rovers a basic path planner is implemented in the system. The path planner works in a sequential fashion, i.e., as long as one rover is moving to reach its final destination the other rovers stay idle. As soon as one rover has reached its final destination the next rover starts its movement. To avoid collision during rover movement, the current and future final positions of the rovers are given to the path planner as obstacles.

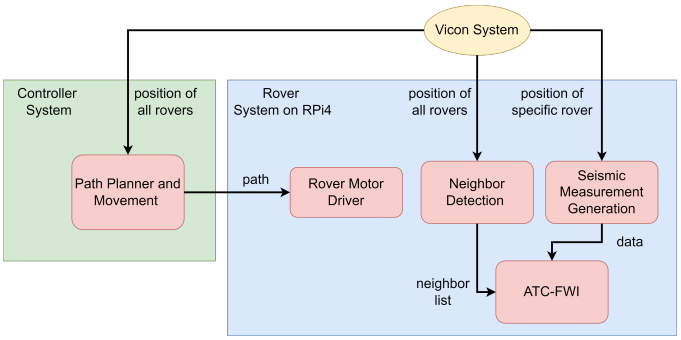

Fig. 1: Overview of the hardware-in-the-loop system architecture. The Rover system runs on a Raspberry Pi 4 while the controller system is on a central PC.

To generate seismic measurements for the rovers we employ a numerical solver of the acoustic wave equation (2). This solver is based on finite differences and provided by the Python package devito [15] that uses highly efficient C++ implementations behind a Python module. It is implemented on the RPi4 modules on the rovers. By solving the wave equation we obtain a 3D acoustic wavefield that is then sampled at the respective rover position $\boldsymbol{x}_r$ to give the measurement data $\boldsymbol{d}_{\mathrm{obs},r}$.

Figure 1 gives an overview of the system architecture. It is divided into three subsystems: The Vicon, the controller and the rover system. The rover system is implemented on the rover's RPi4 performing all the tasks involved for ATC-FWI. The controller system works on a separate computer sending commands to perform ATC-FWI on the rovers. The Vicon system provides both controller and rover system with position data of the rovers in the laboratory environment. The path planner takes the rover positions and designs a path for the rover. In the rover system the positions are used to determine the neighboring rovers with whom a rover can exchange data. This is based on the Euclidean distance between two rovers and a threshold is chosen that determines whether the rover lies in the communication range of the respective rover. Finally, a rover's position is used in the seismic measurement generation that contains the numerical solver of the wave equation. This data is fed into the ATC-FWI together with the neighbor list to perform distributed imaging on a rover.

4. ATC-FWI IMPLEMENTATION DETAILS

In the following, we give details about the implementation of the ATC-FWI on the RPi4 modules carried by the rovers.

For the specific implementation of ATC-FWI, each rover needs to execute the ATC steps (4). To this end, gradients $\boldsymbol{m}_{\Delta,r}$ and intermediate models $\widetilde{\boldsymbol{m}}_r$ need to be exchanged among connected rovers. To realize data exchange over-the-air among the rovers we rely on a central wireless access point that routes the data packets from one rover to the other rovers. By that, we emulate a respective agent-to-agent data exchange in the network. In an ideal scenario, if all rovers initialize the ATC-FWI at the same time they should finish their computation and data exchanges simultaneously. However, this is not given in a real scenario. Therefore, we use a series of flags that synchronize each rover's computation and data transmission with those of its neighbors. The flags used in the ATC-FWI are denoted by *ComputeFlag*, *NextStepFlag* and *IterFlag*. These flags are shared with the neighbors in the form of ROS messages. As soon

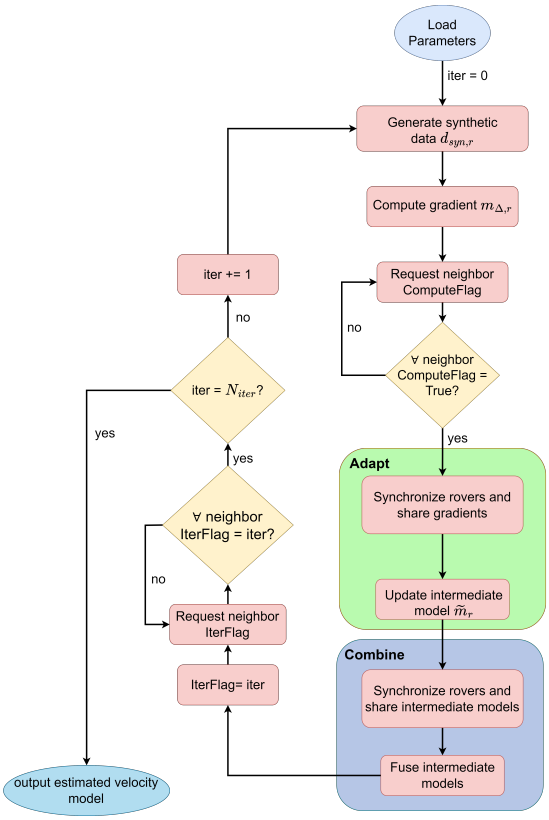

Fig. 2: Flow chart of the ATC-FWI in the HIL implementation.

as the ATC-FWI is performed to obtain the local gradient $\boldsymbol{m}_{\Delta,r}$, the *ComputeFlag* is set high and the rover requests for the flag status from its neighbors. The rover waits until all neighbors have finished their computation. As soon as all the neighbors $\ell \in \mathcal{N}_r$ have obtained their own local gradient $\boldsymbol{m}_{\Delta,\ell}$, the rover synchronizes itself with the neighbors to assure that each of them are at the *adapt* step of the ATC-FWI using the *NextStepFlag*. After synchronization, each rover r requests for the local gradients $\boldsymbol{m}_{\Delta,\ell}$ of its neighbors $\ell \in \mathcal{N}_r$. The rover waits until the local gradients from all the neighbors are received. Then the adapt step (4a) is performed and the intermediate model $\widetilde{\boldsymbol{m}}_r$ is obtained at rover r. The same procedure is executed for the *combine* step (4b). After receiving the intermediate models $\widetilde{\boldsymbol{m}}_\ell$ from all neighbors $\ell \in \mathcal{N}_r$, the rover performs the combine step (4b) to obtain the estimated model $\boldsymbol{m}_r$ which is used to initialize the next iteration. Before the next iteration the rover is synchronized with its neighbors using *IterFlag* to confirm that all the rovers are at the same iteration number. A detailed flow chart of the ATC-FWI implementation is presented in Figure 2.

5. EXPERIMENTS AND RESULTS

We demonstrate the functionality of our proposed implementation of ATC-FWI in the HIL system and show corresponding imaging results. We use an experimental area of $10\,\mathrm{m} \times 5\,\mathrm{m}$ in our lab facilities as exploration area for the rovers. To simulate a seismic exploration this area is scaled up to $500\,\mathrm{m} \times 250\,\mathrm{m}$ and contains a synthetic subsurface model of $500\,\mathrm{m}$ depth. The subsurface model has a constant background velocity of $m_{\mathrm{bg}} = 2\,\mathrm{km/s}$ and contains a cuboidal anomaly in its center with velocity $m_{\mathrm{an}} = 2.5\,\mathrm{km/s}$, cf. Figure 5a.

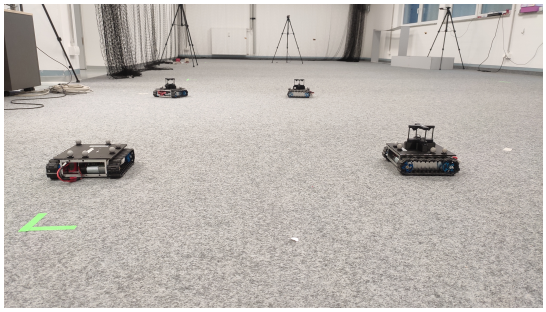

Fig. 3: Rovers used in the HIL system in the laboratory of DLR.

A total of four rovers named *kili, nori, heri* and *uni* are used in the experiments, see Fig. 3. The exploration area is divided into four measurement areas (MAs) as shown in Figure 4. The rovers start in MA1 in a grid formation. Each rover has the same starting model $\boldsymbol{m}_r$ for the subsurface which is a smoothed version of the true model, see Figure 5b. Since FWI is a local optimization scheme and the optimization problem is highly non-convex a good starting model is essential. A seismic source, here a Ricker wavelet, is excited and the rovers measure seismic data generated by the numerical solver at their respective position. Then ATC-FWI is performed for 30 iterations to obtain a subsurface estimate. After that, the rovers move to MA2 where they use the estimated model from MA1 as a starting model to perform again ATC-FWI. This process is repeated for the areas MA3 and MA4. Throughout the experiments the rovers are connected in a circle topology: Each rover has two neighbors as shown in Fig. 4.

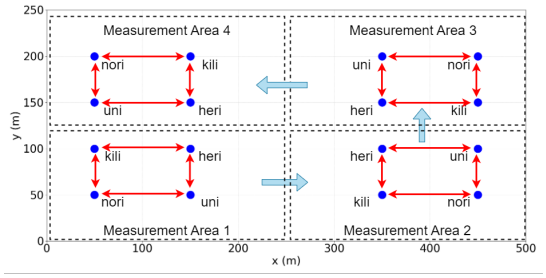

Fig. 4: Rover positions in each measurement area. The red arrows indicate logical connections among the rovers.

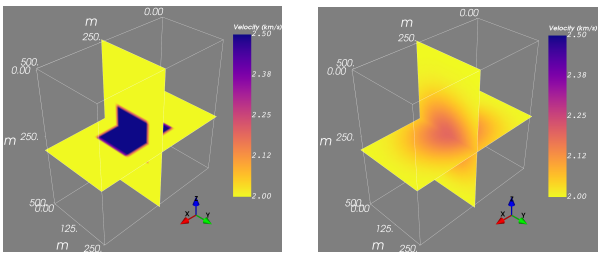

(a) (b)

Fig. 5: (a) True velocity model and (b) starting model for ATC-FWI.

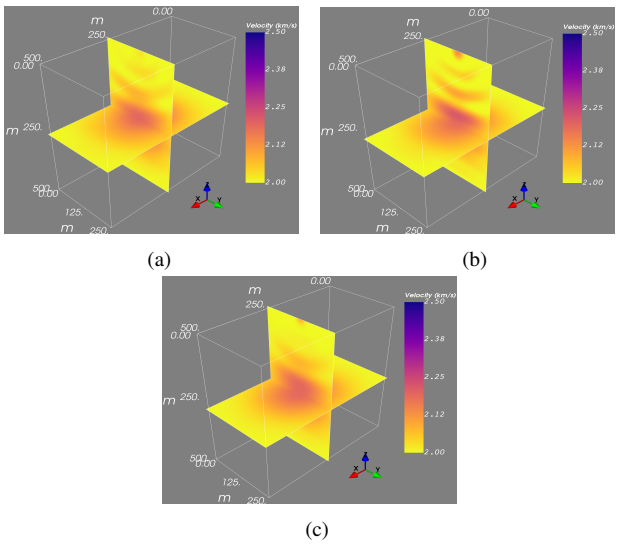

(a) (b) (c)

Fig. 6: Estimated Velocity Model for rover *heri* in ATC-FWI for (a) MA1 and (b) MA4 and (c) benchmark FWI.

Area	MSE			
	heri	*nori*	*uni*	*kili*
MA1	0.00938	0.00938	0.00938	0.00938
MA4	0.00924	0.00924	0.00924	0.00924

Table 1: MSE performance for each rover in MA1 and MA4.

5.1. Source in Center

In this survey, the source is placed at the center of the exploration area in each MA, i.e. at $(250, 125, 0)$ m. Per MA the source is activated once to obtain new measurements. The rovers perform ATC-FWI to image the anomaly in a distributed fashion. Fig. 6a and 6b show the imaging result at rover *heri* for MA1 and MA4. One can observe that the anomaly is imaged more clearly compared to the starting model. Furthermore, the image is enhanced between MA1 and MA4 since more measurements are included into the imaging process. As reference performance we use the centralized FWI with all 16 rover positions over all MAs as receivers that we call *benchmark FWI* in the following. Here, FWI has measurements of all MAs available at once and performs an inversion. The obtained image is shown in Fig. 6c where the anomaly is not as distinct as in MA4 but resembles more the one in MA1.

Table 1 shows the means square error (MSE) of all rovers in MA1 and MA4. The MSE is computed between true and estimated model over all voxels. Each rover obtains similar imaging performance showing that ATC-FWI enables each rover to obtain a global subsurface image locally. Fig. 7a shows the MSE for benchmark FWI, FWI and ATC-FWI over the MAs. FWI follows the same survey procedure as ATC-FWI with the difference of performing centralized imaging in each MA with the measurements of all four rovers. For ATC-FWI the average of the MSE is calculated over all rovers. As observed FWI and ATC-FWI have a high MSE for MA1 while it reduces in the subsequent MAs. This is due the fact that over the MAs the estimated model from the previous MA is used as a starting model for the following one which enhances the imaging. This observation confirms the imaging results from Fig. 6.

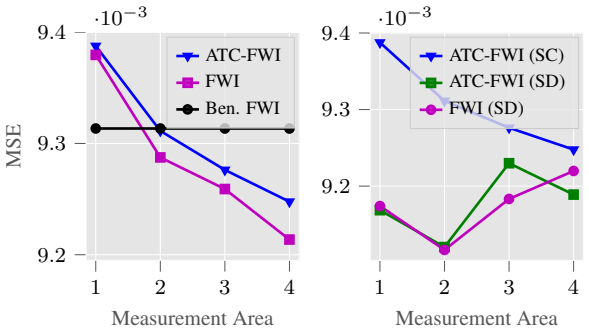

(a) (b)

Fig. 7: MSE performance of surveys where source is placed (a) at the center and (b) diagonal to the rover network.

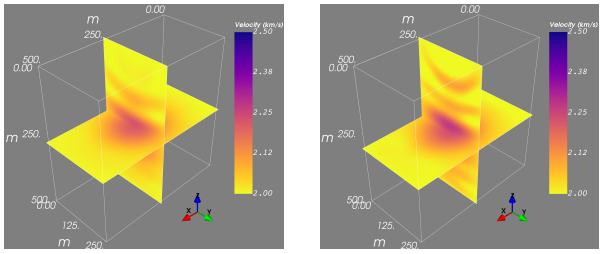

(a) (b)

Fig. 8: Estimated Velocity Model for rover *heri* in ATC-FWI for (a) MA1 and (b) MA4.

5.2. Diagonally Placed Source

Here, he source is always placed diagonally to the rover grid in each MA. This is done to acquire waves that have propagated from the source through the anomaly to the rovers. Fig. 8 shows the results obtained on *heri* in MA1 and MA4. Again one observes better imaging quality of the anomaly in MA4 indicating that the subsurface image is enhanced while progressing over the MAs. Fig. 7b depicts the MSE vs. MAs for ATC-FWI for the survey with the source in the center (SC) and the source diagonally placed (SD). Furthermore, performance of a centralized FWI for the SD survey is shown as reference. The MSE in the SD survey is lower in all the MAs compared to the SC survey. Due to the source-receiver constellation the measured data at the rovers in the SD survey contains more information about the anomaly compared to the one in the SC survey. Hence, the SD survey enables better imaging at the rovers showing that placement of the source has a significant impact on the imaging result. One can also observe that the MSE increases slightly in MA3 and MA4 in the SD survey. Reason for this behavior can be larger artifacts that can be observed especially in the shallow area in Fig. 8b.

6. CONCLUSION

By implementing the ATC-FWI in an HIL system using mobile rovers we took a first step towards robotic seismic surveys envisioned for future planetary missions. We demonstrated that the ATC-FWI is able to image the subsurface locally at each rover via cooperation within the multi-agent network. Furthermore, placement of the source diagonal to the rovers showed better performance compared to a source placed in the center of the exploration area.

7. REFERENCES

[1] David Sollberger, Cedric Schmelzbach, Johan O. A. Robertsson, Nienke Brinkman, Fredrik Andersson, and Sharon Kedar, "Seismic exploration on the Moon, Mars and beyond," in *SEG Technical Program Expanded Abstracts 2020*. Sept. 2020, Society of Exploration Geophysicists.

[2] Brigitte Knapmeyer-Endrun and Taichi Kawamura, "NASA's InSight mission on Mars—first glimpses of the planet's interior from seismology," *Nature Communications*, vol. 11, no. 1, Mar. 2020.

[3] Manfred "Dutch" von Ehrenfried, *Perseverance and the Mars 2020 Mission*, Springer International Publishing, 2022.

[4] Peter Lehner, Sebastian Brunner, Andreas Domel, Heinrich Gmeiner, Sebastian Riedel, Bernhard Vodermayer, and Armin Wedler, "Mobile manipulation for planetary exploration," in *2018 IEEE Aerospace Conference*, Mar. 2018.

[5] Ban-Sok Shin and Dmitriy Shutin, "Subsurface exploration on Mars and Moon with a robotic swarm," in *Global Space Exploration Conference*, 2021.

[6] Emanuel Staudinger, Robert Pöhlmann, Armin Dammann, and Siwei Zhang, "Limits on cooperative positioning for a robotic swarm with time of flight ranging over two-ray ground reflection channel," *Electronics*, vol. 12, no. 9, pp. 2139, May 2023.

[7] Ban-Sok Shin and Dmitriy Shutin, "Adapt-then-combine full waveform inversion for distributed subsurface imaging in seismic networks," in *IEEE ICASSP*, 2021, pp. 4700–4704.

[8] Ban-Sok Shin and Dmitriy Shutin, "Distributed traveltime tomography using kernel-based regression in seismic networks," *IEEE Geoscience and Remote Sensing Letters*, vol. 19, pp. 1–5, 2022.

[9] Albert Tarantola, "Inversion of seismic reflection data in the acoustic approximation," *Geophysics*, vol. 49, no. 8, pp. 1259–1266, 1984.

[10] J. Virieux and S. Operto, "An overview of full-waveform inversion in exploration geophysics," *Geophysics*, vol. 74, no. 6, pp. WCC1–WCC26, Nov. 2009.

[11] Rene Edouard Plessix, "A review of the adjoint-state method for computing the gradient of a functional with geophysical applications," *Geophysical Journal International*, vol. 167, no. 2, pp. 495–503, 2006.

[12] Ali H. Sayed, Shengyuan Tu, Jianshu Chen, Xiaochuan Zhao, and Zaid J Towfic, "Diffusion strategies for adaptation and learning over networks," *IEEE Signal Processing Magazine*, pp. 155–171, 2013.

[13] F.S. Cattivelli and A.H. Sayed, "Diffusion LMS strategies for distributed estimation," *IEEE Transactions on Signal Processing*, vol. 58, no. 3, pp. 1035–1048, Mar. 2010.

[14] Steven Macenski, Tully Foote, Brian Gerkey, Chris Lalancette, and William Woodall, "Robot operating system 2: Design, architecture, and uses in the wild," *Science Robotics*, vol. 7, no. 66, 2022.

[15] M. Louboutin, M. Lange, F. Luporini, N. Kukreja, P. A. Witte, F. J. Herrmann, P. Velesko, and G. J. Gorman, "Devito (v3.1.0): an embedded domain-specific language for finite differences and geophysical exploration," *Geoscientific Model Development*, vol. 12, no. 3, pp. 1165–1187, 2019.